JOURNAL OF THERMOPHYSICS AND HEAT TRANSFER
Vol. 22, No. 2, April–June 2008

Multiphase Nusselt Correlation for Impinging Droplet Heat Flux from a NACA Airfoil

X. Wang*
University of Manitoba, Winnipeg, Manitoba R3T 5V6, Canada
G. F. Naterer†
University of Ontario Institute of Technology, Oshawa, Ontario L1H 7K4, Canada
and
E. Bibeau‡
University of Manitoba, Winnipeg, Manitoba R3T 5V6, Canada

DOI: 10.2514/1.32401

A new nondimensional correlation of convective heat transfer with impinging droplets on a NACA airfoil at varying angles of attack is presented in this paper. An experimental study is performed to develop correlations of heat transfer from a NACA 63-421 airfoil at different angles of attack between 0 to 25 deg and different Reynolds numbers with impinging droplets. A modified Hilpert correlation of convective droplet heat transfer from the NACA airfoil at varying angles of attack is determined with respect to the Reynolds number, Prandtl number, liquid water content, and angles of attack. The modified Hilpert correlation includes the effects of droplet-air interactions on the effective heat transfer coefficient at varying angles of attack. Increasing the angles of attack leads to flow separation and reattachment on the airfoil surface, which affect the structure of the thermal boundary layer and energy exchange, through kinetic energy of impinging droplets and film flow along the surface. The results show that both average and local Nusselt numbers vary with angles of attack. This paper indicates that variations of the air velocity, liquid water content, and angles of attack can be normalized into a modified Hilpert correlation, by using empirical coefficients that involve the chord dimensions, angles of attack, and nondimensional liquid water content.

Nomenclature

C_1, C_2	=	chord coefficients
c	=	chord of airfoil, m
c_m	=	moment center, c/4
D_1, D_2	=	arc angle coefficients
$\bar{h}$	=	average heat transfer coefficient, W/m^2K
h_i	=	local convective heat transfer coefficient, W/m^2K
k	=	thermal conductivity, W/mK
$\overline{Nu}$	=	average Nusselt number
Nu_x	=	local Nusselt number
Pr	=	Prandtl number
Re_c	=	Reynolds number (based on a chord reference length)
T_{in}	=	inner surface temperature of airfoil, °C
T_o	=	outer surface temperature of airfoil, °C
T_∞	=	freestream temperature, °C
W	=	nondimensional liquid water content
α	=	angle of attack
δ	=	thickness of airfoil, m
μ	=	dynamic viscosity of air, kg/ms
ρ	=	density of air, kg/m^3

I. Introduction

AS ONE of the fastest growing sources of renewable energy in the world, wind power has become an important source of energy for the future. In cold climate regions, icing of wind turbines can significantly affect the safety and economics. Numerous wind farms have been built in northern Europe and North America, in areas that have a cold climate and long icing periods in the winter. As a result, it is important to accurately predict the heat transfer from a wind turbine blade in cold climate conditions. Heat transfer characterization is a key component needed to predict power requirements for deicing and thermal mitigation strategies.

Impinging droplet heat transfer at varying angles of attack (AOA) is important to understand icing of wind turbines and airfoil aerodynamics. Numerous past studies have been conducted on forced convection heat transfer from cylinders, plates, and other geometrical configurations. For basic configurations like a flat plate, analytical expressions can be developed for the Nusselt number, in terms of the Reynolds and Prandtl numbers. Empirical correlations based on experimental data are often required for bluff bodies in external flow. In this paper, convective heat transfer from a NACA airfoil is examined at various inclination angles. This paper will develop an extended Hilpert correlation to determine the effects of impinging droplets on the convective heat transfer rate.

Chen [1] examined the heat transfer between a sphere and vertical cylinder with isothermal boundary conditions. The results showed that the average Nusselt number depended on the Raylegh number, ratio of radii, and the cylinder height. Grine et al. [2] used a group of short-wavelength infrared lamps with adjustable power and an infrared camera to measure the heat flux and heat transfer coefficient along a flat plate in a Plexiglass rectangular duct. The experimental data agreed well with analytical predictions, although the authors did not give a correlation of the Nusselt number with respect to the Reynolds number. Zhou and Lee [3] performed experimental studies of heat transfer from a heated flat plate with an impinging air jet. They established how to enhance the heat transfer by adjusting the jet Reynolds number and nozzle-to-plate spacing. Yamamoto et al. [4] developed a predictive model for compressible flow and heat transfer from a NACA-0012 airfoil. Temperature contours around the airfoil, as well as the temperature gradient at the airfoil surface were presented, but the convective heat transfer coefficient was not obtained. Unlike these past studies, this current paper examines the

Received 4 June 2007; revision received 13 November 2007; accepted for publication 24 November 2007.

*Ph.D. Candidate, Department of Mechanical and Manufacturing Engineering.
†Professor and Canada Research Chair in Advanced Energy Systems, Faculty of Engineering and Applied Science, 2000 Simcoe Street North.
‡NSERC/Manitoba Hydro Alternative Energy Industrial Chair, Department of Mechanical and Manufacturing Engineering.

effects of impinging droplets on convective heat transfer from a NACA airfoil at varying angles of attack.

Past studies have acquired experimental data on flow separation and reattachment over an airfoil at different AOA. Amitay and Glezer [5] investigated the reattachment and separation of a flow over a stalled airfoil in a wind tunnel, using surface-mounted synthetic jet actuators. A negative vorticity associated with the separated flow near the leading edge was found in a sequence of smoke visualization images at different angles of attack. Mish and Devenport [6] studied experimentally the effects of mean loading of an airfoil for an unsteady turbulent flow, from 0 to 20 deg angles of attack. The lift and pressure distributions were compared with theoretical results. Hillenherms et al. [7] investigated free and forced oscillations of aerodynamic and structural forces on a 2-D rectangular wing section, from $Re = 1.5 \times 10^6$ to 2.2×10^6, between 0 and 2 deg angle of attack. Decaying and self-sustained pitch oscillations in a forced steady flow were presented and compared at different Reynolds numbers, AOAs, and pitch frequencies. De Bortoli [8] developed a finite volume explicit Runge–Kutta multistage scheme, with a central spatial discretization that combined a multigrid and preconditioning method to simulate flows over NACA-0012 airfoils, including the effects of shock waves. Numerical simulations of an active flow control scheme for airfoils at high Reynolds numbers ($Re_c > 1.2 \times 10^6$) and different angles of attack (8, 12, 22 deg) were performed by Ekaterinaris [9] for a TAU-0015 airfoil using unsteady Reynolds-averaged Navier–Stokes (RANS) equations of incompressible flow. The results showed that flow separation would increase at higher angles of attack. Unlike these studies, this paper will include the effects of impinging droplets on the convective heat transfer analysis. Chen et al. [10] used a copper cylinder head with four 500-W cartridge heaters to investigate the impact of spray parameters on the critical heat flux (CHF) and heat transfer coefficient. The phase transition of freezing droplets in a subzero airstream and freezing time of droplets were presented by Hindmarsh et al. [11]. In this paper, impinging droplets on a NACA airfoil without phase change will be investigated.

In past droplet impact studies, some common geometrical configurations include impinging water droplets on cables and cylinders (Fortin et al. [12], Naterer [13], and Fu et al. [14]). These particular studies involved phase change of impinging droplets. Naterer and Camberos [15] outlined the importance of entropy and the Second Law in multiphase flow predictions with phase change. Other past studies have examined the detailed size and spatial distribution of droplets within spray flows (Hedrih et al. [16], Fuchs and Schickel [17], and Yoon et al. [18]). A dispersed droplet two-phase flow in an icing wind tunnel was examined by Kollár et al. [19]. Phase change of supercooled droplets, mass transfer with evaporation, and sublimation were studied experimentally by Strub et al. [20]. Various experimental methods have been developed to provide detailed insight into the dynamics of droplet motion. Jia and Qiu [21] studied the heat transfer in spray cooling problems, with an experimental heating system, spray system, and droplet characterization method. Sawyer et al. [22] studied a horizontal flat surface under the impact of water droplets to obtain the effects of droplet diameter and collision velocity on the critical heat flux.

Various techniques have been developed to predict coefficients of convective heat transfer from cylinders, airfoils, and other configurations. In this paper, thermocouples embedded within a hollow airfoil (heated internally and cooled externally) will be used to study convective heat transfer with impinging droplets. One-dimensional heat conduction within the thin airfoil surface allows the temperature difference across the surface to give a close approximation of the Fourier conduction flux, which balances the convective heat flux in steady-state conditions. Water droplets are injected into the wind tunnel by a spray bar with an adjustable flow meter. Experimental data will be presented in terms of the Nusselt number, multiphase Reynolds parameter, and modified coefficients of the chord and arc angle. Heat transfer measurements will be obtained at varying Reynolds numbers, liquid water contents, surface positions, and AOAs.

II. Experimental Procedure

The experiments consist of an airflow past a heated NACA-63421 airfoil in a refrigerated wind tunnel (shown in Fig. 1). The test section is a square duct, 91.6 cm in width and 91.6 cm in height. The wall of the test section is transparent, so observations and photographs can be readily obtained. The airfoil is mounted horizontally within the tunnel. The velocity within the wind tunnel reaches up to 42 m/s at temperatures down to −35°C. The velocity is adjusted through an electrical control panel by varying the frequency of the motor, which drives the wind-tunnel fan.

Further details regarding the wind-tunnel setup and associated instrumentation are documented in [23,24]. A prototype airfoil of a wind turbine blade or aircraft wing was fabricated for the experimental studies. A 3-D scanner was used to obtain the NACA profile representation of the airfoil, which was digitized with Geomagic Studio software. The airfoil center is hollow to reduce the weight. Figure 2 shows a chord of the airfoil and the test piece with heater strips and thermocouples. The airfoil chord, span, and thickness are 500, 187.5, and 100 mm, respectively. The airfoil is fabricated with fiberglass and mounted in an aluminum frame inside the test section of the wind tunnel. The thickness of the airfoil fiberglass wall is 3 mm. T-type thermocouples are embedded at both inner and outer edges of the airfoil surface. The thermocouple junctions are mounted flush with each surface at several positions around the airfoil as shown in Fig. 2b. All thermocouple wires are assembled internally within the hollow section of the airfoil. Electrical heater strips are installed along the inner edges of the airfoil. The dimensions of the heating strips are 40 mm in width and 880 mm in length. The operating voltage of the heating strip is 120 V and the power input is 500 W for the experiments. The heater can be adjusted by a variable transformer over a range of voltages

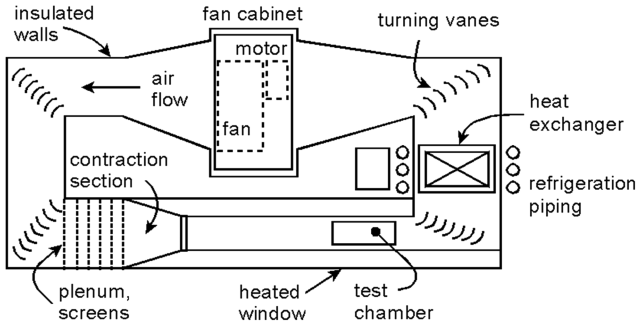

Fig. 1 Top view of refrigerated wind tunnel at the University of Manitoba.

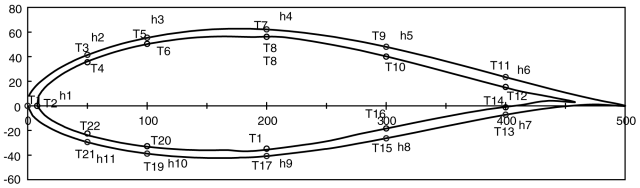

a)

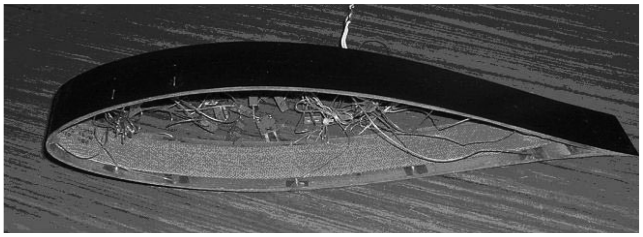

b)

Fig. 2 a) Distribution of measurement points on the test airfoil (dimensions in mm) and b) photograph of the instrumented test airfoil.

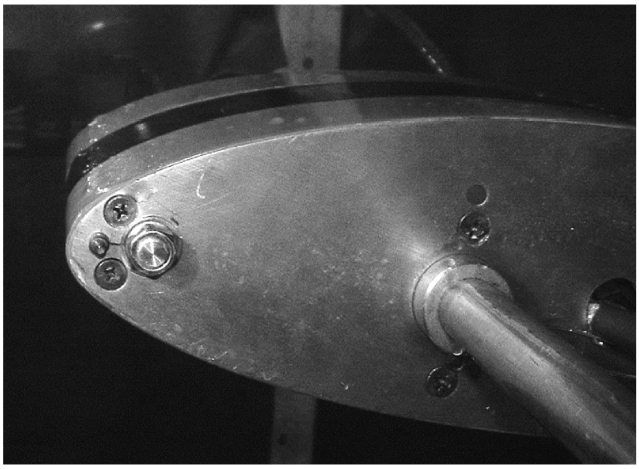

a)

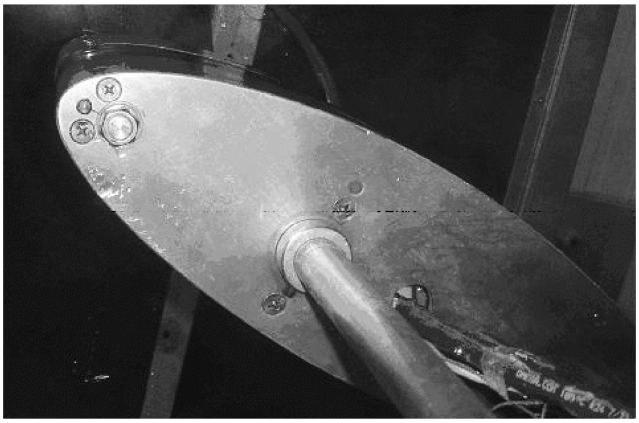

b)

Fig. 3 Photos of the testing airfoil at a) 5 deg and b) 25 deg AOA.

from 0 to 120 V. The heater strips are fastened to the inside of the airfoil with double-sided adhesive tape, after thermocouples are installed. Figure 3 shows different positions of the airfoil in the wind tunnel.

The tests are designed to determine the effects of droplet impact on the convective heat transfer from an airfoil at varying AOA. To study these droplet effects, a spray system was constructed and installed upstream of the test section. The droplet flux from each nozzle was calibrated by controlling the atomizing airflow. Calibrating the mass flow to each nozzle required adjustment of control valves until a uniform flow was obtained. Droplets were emitted conically from the spray bar in parallel streams, which overlapped to create a uniform droplet cloud that impacted on the airfoil surface.

T-type thermocouples are used in a differential connection mode. A direct-reading temperature sensor is used to measure the temperature of the reference junction for cold-junction compensation. The measurement system is controlled by a Labview software program. The experiment uses a total of 25 thermocouples mounted at various locations within the airfoil (see Fig. 2b), including 22 thermocouples installed along the inner and outer surfaces of the airfoil. Temperature differences between inner and outer surfaces are measured at 11 different locations. The thickness of the airfoil is 3 mm, compared to a 500-mm chord and 62.5-mm span, so heat transfer is predominantly one dimensional across the wall of the airfoil. Under steady-state conditions, the heat supplied by the heater is passed through the airfoil wall and transferred to the airstream by convection across the airfoil. Heat conduction through the airfoil is determined from thermocouple measurements within the wall, not the supply of heat input to the wall from the heater, which could be erroneous because of losses through the back side of the heater.

The rate of convective heat transfer from the airfoil is determined by

$$q_{\text{con}} = h(T_o - T_\infty) \tag{1}$$

which can be rearranged to give

$$h = \frac{q_{\text{con}}}{(T_o - T_\infty)} \tag{2}$$

Heater strips below the airfoil surface provide a source of heat input, which is transferred through the thin airfoil surface by conduction, then convection to the external airstream. Heat conduction perpendicular to the surface is much larger than lateral heat conduction, due to the high temperature difference across the thin surface. Thus, the perpendicular Fourier heat flux balances the rate of convective heat transfer to the surrounding airstream, that is,

$$q_{\text{con}} = q_{\text{cd}} = \frac{k(T_{\text{in}} - T_o)}{\delta} \tag{3}$$

Substituting Eq. (2) into Eq. (3), the resulting heat transfer coefficient can be expressed in the following manner:

$$h = \frac{k(T_{\text{in}} - T_o)}{\delta(T_o - T_\infty)} \tag{4}$$

The average coefficient is obtained from spatial averaging around the airfoil:

$$\bar{h} = \frac{1}{s}\int_s h\,\mathrm{d}x = \frac{1}{s}\sum_i^{11} h_i \Delta s_i \tag{5}$$

Then, the average Nusselt number becomes

$$\overline{Nu} = \frac{\bar{h}c}{k_{\text{air}}} \tag{6}$$

The experimental uncertainty of the measured Nusselt number depends on the uncertainty of the local heat transfer coefficient, airfoil chord, thermal conductivity, and geometrical factors. The local heat transfer coefficient depends on the temperature difference between the surface and freestream, as well as the net convective heat loss for each test case. The uncertainty of the measured Reynolds number is estimated as 0.82%, based on the uncertainty of velocity, density of air, viscosity, and bias of the chord length. This measurement uncertainty of the Reynolds number, Re, indirectly affects the uncertainty of the Nusselt number, through the heat transfer coefficient which depends on the air velocity and other parameters. The resulting measurement uncertainty of the Nusselt number was determined to be 7.34%. A detailed analysis of the measurement uncertainties (using the method of Kline and McClintock [25]) is presented in the Appendix.

III. Formulation of Modified Hilpert Correlation

A transition Reynolds number of $Re_c \geq 6 \times 10^5$ characterizes transition to turbulence of the boundary layer over the airfoil. This transition point also occurs for a cylinder, although the transition number for a cylinder in crossflow occurs at $Re_D = 2 \times 10^5$. In this section, experimental data are correlated against the following functional form of the Nusselt number, which is equivalent to the Hilpert correlation for a cylinder in crossflow [26]:

$$\overline{Nu} = cRe^m Pr^{1/3} \tag{7}$$

Over a range of temperatures where the Prandtl numbers are nearly constant, the following reduced form of correlation can be adopted (Van Fossen et al. [27]):

$$\overline{Nu} = ARe^B \tag{8}$$

where A and B are coefficients that depend on flow conditions. This functional form is similar to Nusselt number correlations obtained previously by Wang et al. [28,29] for convective heat transfer from an airfoil at 0-deg AOA. The relationships between Reynolds and

Nusselt number coefficients (c and m) were determined previously based on a least-squares curve fit of measured data by Wang et al. [28,29]. The following correlations were obtained for convective heat transfer from an airfoil at 0-deg angle of attack:

$$\overline{Nu} = 0.0943 Re^{0.636} Pr^{1/3} \quad (\text{for } Re \geq 5 \times 10^5) \tag{9}$$

$$\overline{Nu} = 2.483 Re^{0.389} Pr^{1/3} \quad (\text{for } Re \leq 5 \times 10^5) \tag{10}$$

For different AOA, a similar functional form will be used, but modified to accommodate varying angles of attack. A modified heat transfer correlation will be developed according to the following equations, which are presented for the Nusselt number in low and high Reynolds number cases, respectively:

$$\overline{Nu} = 0.0943(0.75 + 0.017\alpha) Re^{0.636} Pr^{1/3} \quad (\text{for } Re \geq 5 \times 10^5) \tag{11}$$

$$\overline{Nu} = 2.483(0.75 + 0.013\alpha) Re^{0.389} Pr^{1/3} \quad (\text{for } Re \leq 5 \times 10^5) \tag{12}$$

From Eqs. (9–12), the correlations of the Nusselt number can be used to calculate the heat transfer coefficients from 0 to 25 AOA for the airfoil without droplets in the airstream. However, the presence of droplets can significantly alter the heat transfer rate. Past studies of convective droplet heat transfer from NACA airfoils were presented by Wang et al. [30]. Wind-tunnel measurements of the convection coefficients were obtained at varying Reynolds numbers and liquid water content (LWC) values ranging between 0–2 g/m^3. The results showed that the Nusselt number can be correlated through a multiphase Reynolds number. The following equations were obtained by Wang et al. [31] for convective heat transfer with impinging droplets:

$$\overline{Nu} = 2.483(Re(1 + W))^{0.389} Pr^{1/3} \quad (\text{for } Re(1 + W) \leq 6 \times 10^5) \tag{13}$$

$$\overline{Nu} = 0.0943(Re(1 + W))^{0.636} Pr^{1/3} \quad (\text{for } Re(1 + W) > 6 \times 10^5) \tag{14}$$

where

$$W = \frac{\text{LWC}}{\text{LWC}_0} \tag{15}$$

and LWC_0 refers to a reference value of the liquid water content. In the next section, a reference liquid water content of 0.92 and 1.25 g/m^3 are used separately when LWC ranges from 0 to 0.99 g/m^3 and 1 to 2 g/m^3, respectively. Experimental data will be collected and used to extend Eqs. (11–14) to a suitable correlation for convective droplet heat transfer from a NACA airfoil at varying angles of attack.

IV. Results and Discussion

In this section, experimental results will be presented for convective heat transfer from a NACA-63421 airfoil at varying AOA between 0 and 25 deg. The Reynolds number is varied by changing the air velocity in the icing tunnel and air viscosity (by changing the air temperature). The liquid water content is also varied through different spray flow conditions. Within the refrigerated wind tunnel, air temperatures are varied between −30 and 20°C. The liquid water content ranges from 0 to 45 liter/h. Data are collected over a range of temperatures and liquid water contents that yielded uniform normalization of the Nusselt numbers. For example, normalized data collapsed onto a single curve fit at different temperatures, which indicated consistency and provided useful verification that experimental data were collected accurately.

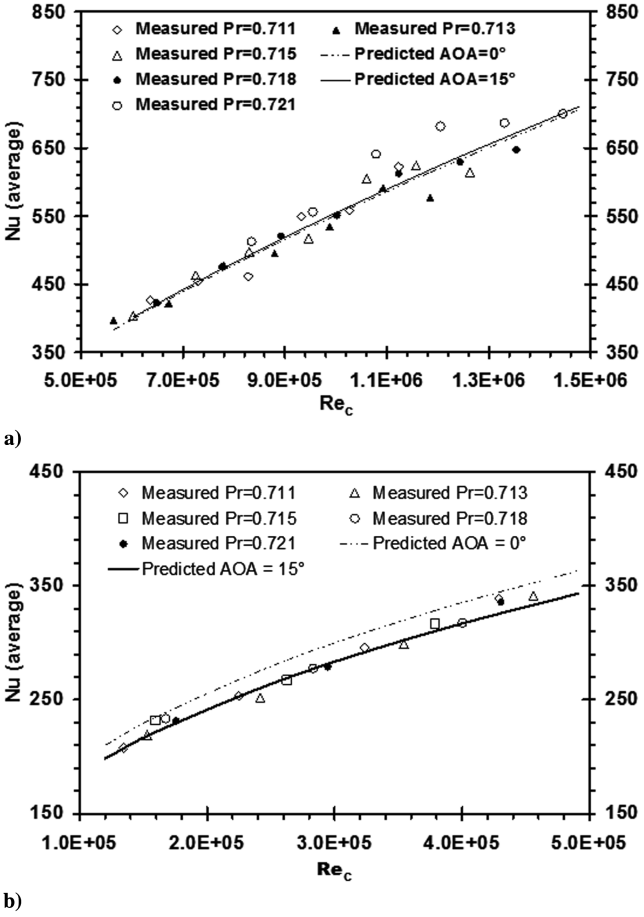

Fig. 4 Measured and predicted Nusselt number at a) high Re_c and b) low Re_c at 15 deg AOA (without LWC).

Particular effort was taken to ensure uniformity of the droplet distribution. Atomizing nozzles were adjusted iteratively with the air and water streams to improve the uniformity. This was a time-consuming process, because they affect each other. Also, particle image velocimetry (PIV) was used to analyze the uniformity of the droplet distribution at each step. Furthermore, icing patterns were observed on the airfoil and the uniformity of ice buildup provided another way to confirm uniformity of the droplet distribution. These efforts and others were taken to provide as uniform a droplet distribution as possible.

From the manufacturer's specifications of the spray nozzles, the droplet size is 100 μm. At the nozzle exit, droplet ejection is air assisted because the airstream drives the emission from the nozzle, rather than ejection at a particular velocity, so the droplet velocity is close to the airstream velocity. Droplet sizes are controlled by variations of air pressure. The air atomizing nozzles can produce a reliable spray pattern with water mean droplet diameters ranging between 10 and 1000 μm.

Figure 4 compares the measured data and correlations for both high and low Reynolds numbers at a 15-deg angle of attack without LWC. The results illustrate that the average Nusselt number increases at a higher Reynolds number. Measured data at varying temperatures (different Prandtl numbers) are illustrated in the figure. For the low Reynolds number, without the AOA correction factors developed in the previous section, the zero AOA correlation would overpredict the measured data across the range of Reynolds numbers. The AOA correction [see Eqs. (11) and (12) for high and low Reynolds number cases, respectively] to the Hilpert correlation was determined empirically from the curve fit of measured data.

Results of measured data at different values of the liquid water content are plotted in Fig. 5, together with a correlated curve fit of experimental data without water droplets, which was derived by conducting the experiments at the same operating AOA, but with the

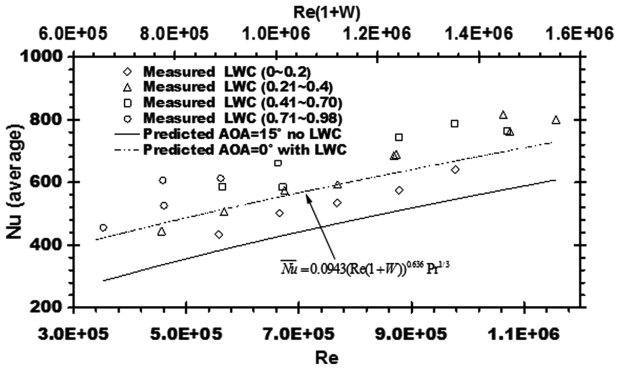

Fig. 5 Comparison of measured data with LWC and Nusselt number correlations without LWC at 15 deg AOA, as well as the predicted Nusselt number correlation with LWC at 0 deg AOA.

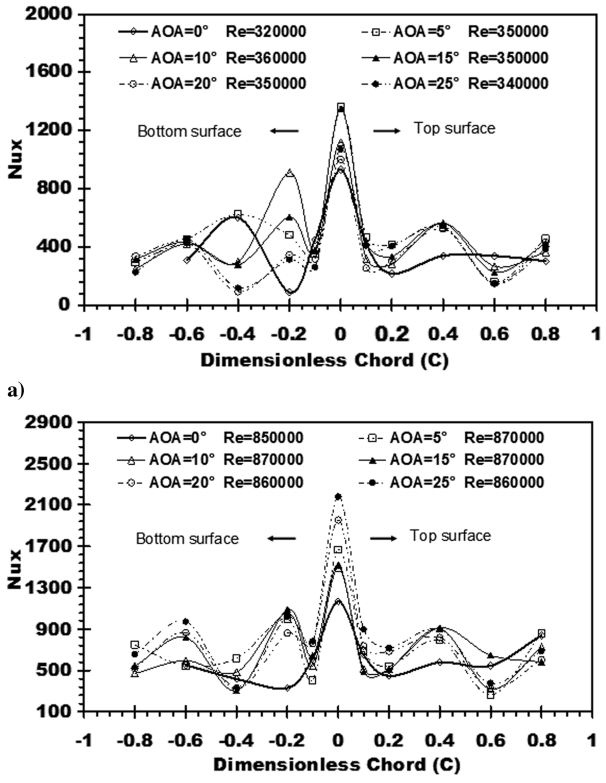

Fig. 6 Nusselt number at a) low and b) high Reynolds numbers with LWC at varying AOA.

spray nozzles closed. In Fig. 5, the solid curve represents empirical correlations without droplets when $\alpha(\mathrm{AOA}) = 15$ deg. The markers correspond to measured data with droplets at 15-deg AOA and the dotted line illustrates predictions of the Nusselt number with the multiphase Reynolds parameter, $Re(1 + W)$. The curve of Eq. (15) in Fig. 5 has a higher Reynolds number, due to the data modification by $(1 + W)$. Neither the correlation of the Nusselt number and the Reynolds number in Eq. (11), nor Eq. (14), can be used to predict the heat transfer correlation with liquid water droplets at varying AOA, although the multiphase Reynolds number can be used to include effects on the heat transfer coefficient. A new heat transfer correlation is needed in this situation. The experimental data indicate that the average Nusselt number at a fixed AOA rises about 26.4% for $Re_c \geq 6 \times 10^5$, when water droplets are introduced into the airstream. Impinging droplets enhance the rate of heat exchange between the surface and airstream, as they enhance fluid mixing along the wall, thereby increasing the convective heat exchange and Nusselt number.

Experimental results show that the angle of attack substantially affects the heat transfer coefficient, both with and without water droplets. Figure 6 shows the measured local Nusselt numbers, Nu_x, at different positions with a LWC of 0.58 and 0.75 g/m^3 at high and low Reynolds numbers. The stagnation point is located at $x/C = 0$. The curve with $\mathrm{AOA} = 0$ shows that the Nusselt number decreases after the stagnation point, due to the thickening boundary layer along the top and bottom surfaces. It falls to the lowest point at the position of $0.2c$ along the chord of the airfoil, and then it increases thereafter. Although both surfaces of the airfoil have the same trends near the leading edge of the airfoil, the lowest value of Nu_x occurs along the bottom surface.

The surface would have the same local Nusselt number if the airfoil was symmetric in shape and orientation with respect to the freestream, but nonsymmetry leads to different Nusselt number results on each side of the stagnation point. The thickness of the laminar boundary layer increases when x increases from the leading edge to the trailing edge. At some point along each surface, the boundary layer transition occurs and the boundary layer becomes turbulent. In the laminar region, the heat transfer coefficient decreases when the thickness of the boundary layer increases. The heat transfer coefficient increases when the boundary layer becomes turbulent.

In Fig. 6a, it can be observed how the local Nusselt number changes with AOA at $\mathrm{LWC} = 0.75$ g/m^3, for cases of low Reynolds numbers. At the stagnation point, the Nusselt number changes with LWC. Without droplets in the airstream, it remains nearly uniform at different values of AOA, whereas the Nusselt number increases higher than $\mathrm{AOA} = 0$ with a nonzero LWC, although it does not depend on the angle of attack. It also changes significantly with AOA along the chord of the airfoil. The Nusselt number decreases at $\pm 0.1c$, $-0.4c$, $0.6c$ and it significantly increases at $-0.2c$, $-0.6c$ and $+0.4c$ and $+0.8c$. Figure 6b shows the Nusselt number results for cases of high Reynolds numbers at various AOA and $\mathrm{LWC} = 0.51$ g/m^3. At angles of attack of 5 deg, the local Nusselt number at the stagnation point is lower than the case for 20 and 25 deg, but higher than the case for 10 and 15 deg.

Also, all values of the Nusselt number at the stagnation point are higher than the case for 0-deg AOA. Values of the Nusselt number at $-0.1c$, $+0.1c$, and $+0.6c$ change depending on the AOA at those points. The values at $-0.2c$, $-0.6c$, $+0.2c$, and $+0.4c$ are higher than an AOA of zero at the same points. As AOA increase, the changes of the local Nusselt number with AOA become more pronounced at higher Reynolds numbers. The Nusselt number at the stagnation point is higher than the value of Nu at the stagnation point, when the angle of attack is 0 deg. Also, no points of the local Nusselt number along the chord of the airfoil have lower values than the Nusselt number at 0 deg for the same points. Furthermore, Nu_x for the other points along the chord of the airfoil are larger than the values at the same points for 0 deg. The average Nusselt number is expected to have similar trends at high multiphase Reynolds numbers.

The movement of the point of separation depends on the adverse pressure gradient, angle of attack, and Reynolds number [32]. When the Reynolds number increases, the separation point moves toward the leading edge. Higher turbulence over the airfoil will enhance the heat transfer at higher Reynolds numbers. Okong'o and Knight [33] predicted 2-D laminar flow over a pitched airfoil, by using a second-order discretization with Roe's method. At a larger Reynolds number, a primary recirculation region forms closer to the leading edge at Mach numbers of 0.2 and 0.5. When the AOA varies from 14.5 to 22.5 deg, the air motion over a NACA-0012 airfoil generated a flow reversal at 14.5 deg. The primary recirculation region formed at 16.5 deg. The primary recirculation region with critical points formed at 19.5 deg, while the secondary recirculation region with critical points and primary recirculation occurred at 21 deg. A tertiary recirculation region with secondary recirculation and critical points occurred at 22.5 deg. This implies that a recirculation region developed and moved toward the leading edge, when the angle of attack increased.

The results also showed that a higher Reynolds number will lead to a circulation region at the smaller angle of attack, while the center of recirculation moves forward to the leading edge. These mechanisms

of the recirculation zone affect the convective heat exchange, so the Nusselt correlation requires a suitable dependence on AOA, which reflects the physical processes in the boundary layer. A modified Hilpert correlation is used to fit measured data obtained from the experiments according to Eqs. (11–14) as follows:

$$\overline{Nu} = 2.483(C_1 + D_1\alpha)(Re(1+W))^{0.389}Pr^{1/3}, \quad \text{for } Re(1+W) \le 6\times 10^5 \tag{16}$$

and

$$\overline{Nu} = 0.0943(C_2 + D_2\alpha)(Re(1+W))^{0.636}Pr^{1/3}, \quad \text{for } Re(1+W) \ge 6\times 10^5 \tag{17}$$

where α, C_1, C_2, D_1, and D_2 refer to the angle of attack and coefficients used as correction factors for the correlations developed in the limiting case of zero angle of attack. The normalized chord of the airfoil c and dynamic center c_m are used to define the first coefficient, $C_1 = 1 - c_m/c = 1 - 0.25/1 = 0.75$. The remaining coefficients are found from a unit angle and exchange factor from 1 deg to the maximum arclength: $\pi/180 = 0.017$ and $D_1 = C_1^2 \times 0.017 = 0.01$. These coefficients aim to provide a functional expression that accounts for movement of the point of separation along the airfoil surface, due to the varying angle of attack. By including the AOA correction factor based on this movement, the expected Nusselt number trends for varying angles of attack can be established for the heat transfer correlation.

The coefficient D_2 must be modified differently by D_1 and C_1, for cases of higher turbulence to decrease the effect of the angle of attack under conditions of impinging droplets. Movement of the transition point changes at high Reynolds numbers, so $D_2 = C_1 \times D_1 = 0.007$. The other coefficient is $C_2 = c/c = 1$. Higher turbulence increases the heat transfer coefficient in droplet flow conditions, regardless of the angle of attack. Using the resulting factors in Eqs. (16) and (17), the following correlations are obtained for the Nusselt number in low and high Reynolds number cases, respectively,

$$\overline{Nu} = 2.483(0.75 + 0.01\alpha)(Re(1+W))^{0.389}Pr^{1/3} \quad \text{for } Re(1+W) \le 6\times 10^5 \tag{18}$$

$$\overline{Nu} = 0.0943(1 + 0.007\alpha)(Re(1+W))^{0.636}Pr^{1/3} \quad \text{for } Re(1+W) \ge 6\times 10^5 \tag{19}$$

Figure 7 compares the measured data and predictions at AOA = 15 deg, when the above corrections factors are applied to the Nusselt number correlation. Measured data at varying temperatures (different Prandtl numbers) are illustrated in Fig. 7 by using the multiphase Reynolds parameter. Without the previous correction factors, the zero AOA correlation would overpredict the measured data across the range of Reynolds numbers. For the results in Fig. 7, the curve regression coefficient is $R^2 = 0.961$. Without the multiphase Reynolds parameter, a consistent trend could not be observed with the data. But the definition of $Re(1+W)$ and modification for the angles of attack allow an effective normalization of measured data. The correlation incorporates effects of both Reynolds number and LWC, thereby reducing the number of independent variables in plotted figures.

Figure 8 shows additional results for other angles of attack: 5, 10, 15, 20, and 25 deg at the higher Reynolds number. In each case, the correction factors for Nusselt number correlations have yielded good agreement between the predicted and measured data. The Nusselt number increases at higher angles of attack, because the separation point moves upstream, induces turbulence, and enhances heat exchange between the surface and fluid. At lower Reynolds numbers, close agreement is also achieved, both at 15 deg in Fig. 9 and higher angles of attack in Fig. 10. As observed previously for higher Reynolds numbers, the Nusselt number increases at higher angles of

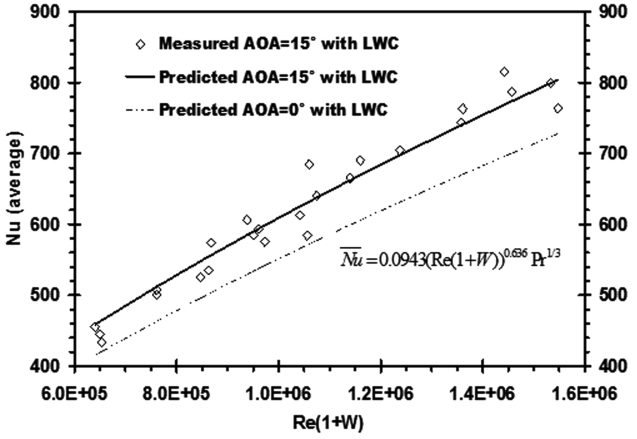

Fig. 7 Predicted and measured Nusselt number with droplets for $Re(1+W) \ge 600,000$ at 15° AOA.

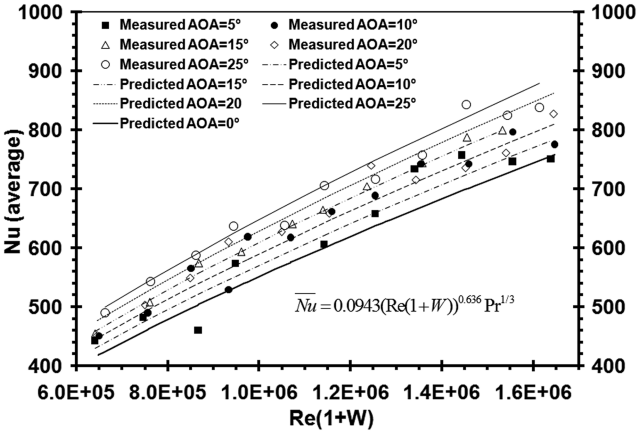

Fig. 8 Measured date and predicted Nusselt number with droplets at varying AOA for high $Re(1+W)$.

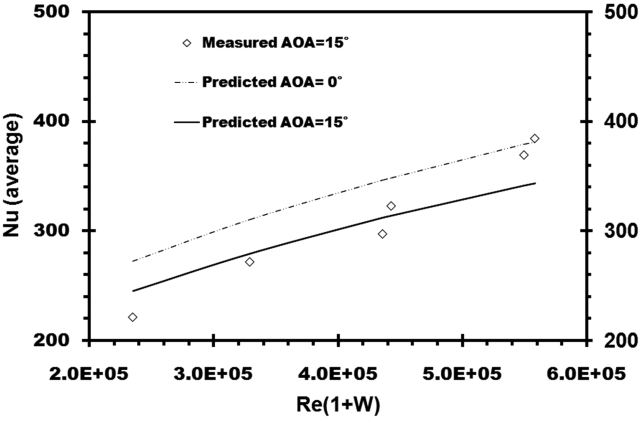

Fig. 9 Predicted and measured Nusselt number with droplets for $Re(1+W) < 600,000$ at 15 deg AOA.

attack. The results indicate that a standard Hilpert form of convection correlation can be used to predict heat transfer from a NACA airfoil at varying angles of attack. A correction factor on a standard Hilpert correlation has yielded relatively close agreement with measured data of the Nusselt number. In Eq. (18), we find the factor to modify the correlation is $0.75 + 0.01\alpha$. The value is 1 when $\alpha = 25$. Equation (13) (published in [31]) is presented for AOA = 0. Heat transfer from the airfoil varies with AOA, so when $\alpha = 25$, Eq. (18) becomes the same as Eq. (13).

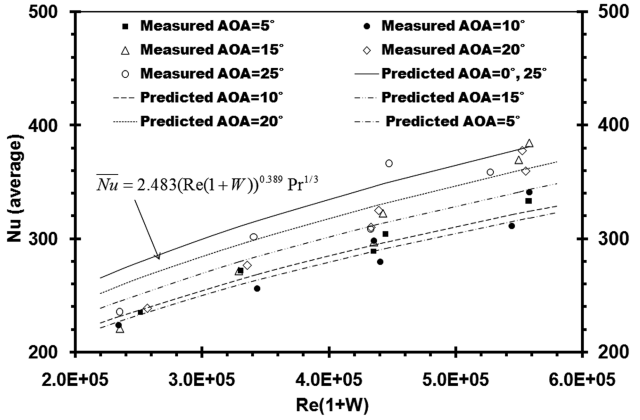

Fig. 10 Predicted and measured Nussulet number with droplets for $Re(1+W) < 600,000$ at varying AOA.

Despite experimental variability of measured data, the correlated results indicate that the correction factor $(1 + 0.007\alpha)$ provides a useful improvement over the zero AOA correlation. In Figs. 5–8, the experimental data exhibited a significant difference with the zero AOA correlation, wherein the measured values are notably larger than correlated values at zero AOA. The modified correlation with a dependence on AOA was shown to demonstrate the proper trends at varying AOA. The empirical factor in the modified correlation varies with AOA, unlike previous correlations with a constant value. The results have shown close agreement between the experimental and correlated Nusselt number values over a range of multiphase Reynolds numbers.

V. Conclusions

This article has presented an experimental study of heat transfer coefficients for forced convection with droplet impact on a NACA-63421 airfoil at varying angles of attack from 0 to 25 deg. Wind-tunnel studies were conducted at varying wind speeds and LWC values ranging between 0–2 g/m^3. The experimental data were correlated with respect to the Nusselt number, angle of attack, and a newly defined multiphase Reynolds number. Both average and local Nusselt numbers are obtained and nondimensionalized in a modified Hilpert correlation. The modifications of AOA are $(0.75 + 0.01\alpha)$ and $(1 + 0.007\alpha)$ separately for low and high multiphase Reynolds numbers, respectively. An uncertainty analysis yielded an experimental uncertainty of 7.34% for the measured Nusselt numbers. It was shown that the functional form of the Hilpert correlation can effectively accommodate measured data for the NACA airfoil over a range of Reynolds numbers at various AOA.

Appendix: Measurement Uncertainties

In this Appendix, the method of Kline and McClintock [25] is used to estimate the measurement uncertainties in the reported experiments. From Eq. (4), the heat transfer coefficient was determined as follows:

$$h = \frac{k(T_{\mathrm{in}} - T_o)}{\delta(T_o - T_\infty)} \tag{A1}$$

In the experiments, the parameters T_o, T_{in}, T_∞, and δ were measured. The total uncertainty U_h includes a precision uncertainty P_h, and B_h (precision and bias limits for each variable and parameter contribution to the uncertainty), where

$$U_h = \sqrt{P_h^2 + B_h^2} \tag{A2}$$

The precision contribution can be calculated from the following equation:

$$P_h^2 = \left(\frac{\partial h}{\partial T_{\mathrm{in}}}\right)^2 P_{T\mathrm{in}}^2 + \left(\frac{\partial h}{\partial T_o}\right)^2 P_{To}^2 + \left(\frac{\partial h}{\partial T_\infty}\right)^2 P_{T\infty}^2 + \left(\frac{\partial h}{\partial \delta}\right)^2 P_\delta^2 + \left(\frac{\partial h}{\partial k}\right)^2 P_k^2 \tag{A3}$$

Equation (A3) is divided by Eq. (A1) and rearranged as follows:

$$\left(\frac{P_h}{h}\right)^2 = \left(\frac{P_{T\mathrm{in}}}{\Delta T_1}\right)^2 + \left(\frac{P_{To}}{\Delta T_2}\right)^2 + \left(\frac{P_{T\infty}}{\Delta T_2}\right)^2 + \left(\frac{P_\delta}{\delta}\right)^2 + \left(\frac{P_k}{k}\right)^2 \tag{A4}$$

where $\Delta T_1 = T_{\mathrm{in}} - T_o$, and $\Delta T_2 = T_o - T_\infty$.

Using a similar analysis, the bias contribution can be obtained as

$$\left(\frac{B_h}{h}\right)^2 = \frac{B_{T\mathrm{in}}^2 + B_{To}^2 - 2B'_{T\mathrm{in}}B'_{To}}{\Delta T_1^2} + \frac{B_{To}^2 + B_{T\infty}^2 - 2B'_{To}B'_{T\infty}}{\Delta T_2^2} + \frac{2}{\Delta T_1 \Delta T_2} B_{To}^2 - \frac{2}{\Delta T_1 \Delta T_2} B'_{To}B'_{T\mathrm{in}} + \frac{2}{\Delta T_1 \Delta T_2}(B'_{T\infty}B''_{T\mathrm{in}} - B'_{To}B'_{T\infty}) + \frac{B_k^2}{k^2} + \frac{B_\delta^2}{\delta^2} \tag{A5}$$

$$\left(\frac{B_h}{h}\right)^2 = \frac{B_{T\mathrm{in}}^2}{\Delta T_1^2} + \left(\frac{1}{\Delta T_1} + \frac{1}{\Delta T_2}\right)B_{To}^2 - 2\left(\frac{1}{\Delta T_1^2} + \frac{1}{\Delta T_1 \Delta T_2}\right)B'_{To}B'_{T\mathrm{in}} + \frac{2}{\Delta T_1 \Delta T_2} B'_{T\infty}B'_{T\mathrm{in}} - 2\left(\frac{1}{\Delta T_2^2} + \frac{1}{\Delta T_1 \Delta T_2}\right)B'_{To}B'_{T\infty} + \frac{B_{T\infty}^2}{\Delta T_2^2} + \frac{B_k^2}{k^2} + \frac{B_\delta^2}{\delta^2} \tag{A6}$$

where $B'_{T\mathrm{in}}$, B'_{To} and $B'_{T\infty}$ are the portions of $B_{T\mathrm{in}}$, B_{To} and $B_{T\infty}$, respectively, which arise from an identical error source, so they are assumed to be perfectly correlated. The bias contribution to the uncertainty is reduced to

$$\left(\frac{B_h}{h}\right)^2 = \frac{B_k^2}{k^2} + \frac{B_\delta^2}{\delta^2} \tag{A7}$$

The total uncertainty of the heat transfer coefficient becomes

$$\frac{U_h}{h} = \sqrt{\left(\frac{P_h}{h}\right)^2 + \left(\frac{B_h}{h}\right)^2} \tag{A8}$$

In this paper, temperatures were measured 100 times per second and 10-s average values were calculated, so $P_{T\mathrm{in}} = P_{To} = P_{T\infty} =$ 0.64 K. Additional variables are $\Delta T_1 = 10.25$ K, $\Delta T_2 = 42.42$ K, $P_\delta = 0.095$ mm, $\delta = 2.999$ mm, and $B_\delta = 0.005$ mm. It was assumed that $P_h/k = 0$ and $B_k/k = 0$. Hence, the uncertainty of the heat transfer coefficient becomes $U_h = 7.23\%$.

For the Nusselt number in the experiments, $\overline{Nu} = \bar{h}c/k$, and the total uncertainty can be expressed in the following manner:

$$\frac{U_{\overline{Nu}}}{\overline{Nu}} = \sqrt{\left(\frac{P_{\overline{Nu}}}{\overline{Nu}}\right)^2 + \left(\frac{B_{\overline{Nu}}}{\overline{Nu}}\right)^2} = \sqrt{\left(\frac{U_h}{h}\right)^2 + \left(\frac{B_c}{c}\right)^2 + \left(\frac{B_k}{k}\right)^2} = \sqrt{0.00723^2 + \left(\frac{0.5}{498.5}\right)^2 + 0.005^2} = 7.34\% \tag{A9}$$

where it has been assumed that $B_k/k = 0.5\%$.

The measurement uncertainty of the average freestream velocity was

$$\frac{U_u}{u} = \sqrt{\left(\frac{1}{2}\frac{U_{\rho_l}}{\rho_l}\right)^2 + \left(\frac{1}{2}\frac{U_{\rho_{\mathrm{air}}}}{\rho_{\mathrm{air}}}\right)^2 + \left(\frac{1}{2}\frac{B_{\Delta h}}{\Delta h}\right)^2} = \sqrt{\left(\frac{1}{2}\times 0.005\right)^2 + \left(\frac{1}{2}\times\frac{0.005}{1.371}\right)^2 + \left(\frac{1}{2}\times 0.005\right)^2} \tag{A10}$$

which yields an uncertainty of 0.397%. The uncertainties of the tabulated density of air and manometer fluid for the pitot tube measurements of velocity are

$$\frac{U_{\rho_l}}{\rho_l} = \frac{U_{\rho_{\text{air}}}}{\rho_{\text{air}}} = 0.5\% \tag{A11}$$

The uncertainties of Reynolds and Nusselt numbers become 0.818 and 7.34%, respectively, based on the uncertainty of velocity, density of air, viscosity, and bias of chord length.

Acknowledgments

Financial support from the Natural Sciences and Research Council of Canada (NSERC), Manitoba Hydro, and the Canada Foundation for Innovation (CFI) are gratefully acknowledged.

References

[1] Chen, W. R., "A Numerical Study of Laminar Free Convection Heat Transfer Between Inner Sphere and Outer Vertical Cylinder," *International Journal of Heat and Mass Transfer*, Vol. 50, Nos. 13–14, 2007, pp. 2656–2666. doi:10.1016/j.ijheatmasstransfer.2006.11.046

[2] Grine, A., Saury, D., Desmons, J. Y., and Harmand, S., "Identification Models for Transient Heat Transfer on a Flat Plate," *Experimental Thermal and Fluid Science* (to be published).

[3] Zhou, D. W., and Lee, S., "Forced Convective Heat Transfer with Impinging Rectangular Jets," *International Journal of Heat and Mass Transfer*, Vol. 50, No. 9, 2007, pp. 1916–1926. doi:10.1016/j.ijheatmasstransfer.2006.09.022

[4] Yamamoto, S., Niiyama, D., and Shin, B. R., "A Numerical Method for Natural Convection and Heat Conduction Around and in a Horizontal Circular Pipe," *International Journal of Heat and Mass Transfer*, Vol. 47, No. 26, 2004, pp. 5781–5792. doi:10.1016/j.ijheatmasstransfer.2004.06.039

[5] Amitay, M., and Glezer, A., "Controlled Transients of Flow Reattachment over Stalled Airfoils," *International Journal of Heat and Fluid Flow*, Vol. 23, No. 5, 2002, pp. 690–699. doi:10.1016/S0142-727X(02)00165-0

[6] Mish, P. F., and Devenport, W. J., "An Experimental Investigation of Unsteady Surface Pressure on an Airfoil in Turbulence—Part 1: Effects of Mean Loading Periodical," *Journal of Sound and Vibration*, Vol. 296, No. 3, 2006, pp. 417–446. doi:10.1016/j.jsv.2005.08.008

[7] Hillenherms, C., Schröder, W., and Limberg, W., "Experimental Investigation of a Pitching Airfoil in Transonic Flow," *Aerospace Science and Technology*, Vol. 8, No. 7, 2004, pp. 583–590. doi:10.1016/j.ast.2004.07.001

[8] De Bortoli, A. L., "Multigrid Based Aerodynamical Simulations for the NACA 0012 Airfoil," *Applied Numerical Mathematics*, Vol. 40, No. 1, 2002, pp. 337–349. doi:10.1016/S0168-9274(01)00081-2

[9] Ekaterinaris, J. A., "Prediction of Active Flow Control Performance on Airfoils and Wings," *Aerospace Science and Technology*, Vol. 8, No. 5, 2004, pp. 401–410. doi:10.1016/j.ast.2004.02.003

[10] Chen, R. H., Chow, L. C., and Navedo, J. E., "Effects of Spray Characteristics on Critical Heat Flux in Subcooled Water Spray Cooling," *International Journal of Heat and Mass Transfer*, Vol. 45, No. 19, 2002, pp. 4033–4043. doi:10.1016/S0017-9310(02)00113-8

[11] Hindmarsh, J. P., Russell, A. B., and Chen, X. D., "Experimental and Numerical Analysis of the Temperature Transition of a Suspended Freezing Water Droplet," *International Journal of Heat and Mass Transfer*, Vol. 46, No. 7, 2003, pp. 1199–1213. doi:10.1016/S0017-9310(02)00399-X

[12] Fortin, G., Laforte, J. L., and Ilinca, A., "Heat and Mass Transfer During Ice Accretion on Aircraft Wings with an Improved Roughness Model," *International Journal of Thermal Sciences*, Vol. 45, No. 6, 2006, pp. 595–606. doi:10.1016/j.ijthermalsci.2005.07.006

[13] Naterer, G. F., "Temperature Gradient in the Unfrozen Liquid Layer for Multiphase Energy Balance with Incoming Droplets," *Journal of Heat Transfer*, Vol. 125, No. 1, 2003, pp. 186–189. doi:10.1115/1.1532015

[14] Fu, P., Farzaneh, M., and Bouchard, G., "Two-Dimensional Modelling of Ice Accretion Process on Transmission Line Wires and Conductors," *Cold Regions Science and Technology*, Vol. 46, No. 2, 2006, pp. 132–146. doi:10.1016/j.coldregions.2006.06.004

[15] Naterer, G. F., and Camberos, J. A., "Entropy and the Second Law in Fluid Flow and Heat Transfer Simulation," *Journal of Thermophysics and Heat Transfer*, Vol. 17, No. 3, July 2003, pp. 360–371.

[16] Hedrih, K., Babović, V., and Šarković, D., "An Auxiliary Size Distribution Model for the Ultrasonically Produced Water Droplets," *Experimental Thermal and Fluid Science*, Vol. 30, No. 6, 2006, pp. 559–564. doi:10.1016/j.expthermflusci.2005.12.001

[17] Fuchs, W., and Schickel, K. P., "Aircraft Icing in Visual Meterological Conditions Below Low Stratus Clouds," *Atmospheric Research*, Vol. 36, 1995, pp. 339–345. doi:10.1016/0169-8095(94)00046-G

[18] Yoon, S. S., DesJardin, P. E., Presser, C., Hewson, J. C., and Avedisian, C. T., "Numerical Modeling and Experimental Measurements of Water Spray Impact and Transport over a Cylinder," *International Journal of Multiphase Flow*, Vol. 32, No. 1, 2006, pp. 132–157. doi:10.1016/j.ijmultiphaseflow.2005.05.007

[19] Kollár, L. E., Farzaneh, M., and Karev, A. R., "Modeling Droplet Collision and Coalescence in an Icing Wind Tunnel and the Influence of These Processes on Droplet Size Distribution," *International Journal of Multiphase Flow*, Vol. 31, No. 1, 2005, pp. 69–92. doi:10.1016/j.ijmultiphaseflow.2004.08.007

[20] Strub, M., Jabbour, O., Strub, F., and Bédécarrats, J. P., "Experimental Study and Modeling of the Crystallization of a Water Droplet," *International Journal of Refrigeration*, Vol. 26, 2003, pp. 59–68. doi:10.1016/S0140-7007(02)00021-X

[21] Jia, W., and Qiu, H. H., "Experimental Investigation of Droplet Dynamics and Heat Transfer in Spray Cooling," *Experimental Thermal and Fluid Science*, Vol. 27, No. 7, 2003, pp. 829–838. doi:10.1016/S0894-1777(03)00015-3

[22] Sawyer, M. L., Jeter, S. M., and Abdel-Khaliks, S. I., "A Critical Heat Flux Correlation for Droplet Impact Cooling," *International Journal of Heat and Mass Transfer*, Vol. 40, No. 9, 1997, pp. 2123–2131. doi:10.1016/S0017-9310(96)00267-0

[23] Naterer, G. F., Popplewell, N., Barrett, W., Anderson, J., Faraci, E., McCartney, D., and Lehmann, W., "Experimental Facility for New Hybrid Ice/Spray Flow Tunnel with Laser Based Droplet Measurement," AIAA Paper 2002-2867, 24–27 June 2002.

[24] Wang, X., Naterer, G. F., and Bibeau, E., "Experimental Study of 3-D Blades and Wind Turbines Under Icing Conditions," *International Green Energy Conference*, University of Ontario Institute of Technology, Oshawa, Canada, 25–29 June 2006.

[25] Kline, S. J., and McClintock, F. A., "Describing Uncertainties in Single-Sample Experiments," *Mechanical Engineering*, Vol. 75, 1953, pp. 3–8.

[26] Incropera, F. P., and deWitt, D. P., *Fundamentals of Heat and Mass Transfer*, 4th ed., Wiley, New York, 1996, Chap. 7.

[27] Van Fossen, G. J., Simoneau, R. J., Olsen, W. A., and Shaw, R. J., "Heat Transfer Distributions Around Nominal Ice Accretion in the LEWIS Icing Research Tunnel," AIAA Paper 84-0017, 1984.

[28] Wang, X., Bibeau, E., and Naterer, G. F., "Experimental Correlation of Forced Convection Heat Transfer from a NACA Airfoil," *Experimental Thermal and Fluid Science* (to be published).

[29] Wang, X., Bibeau, E., and Naterer, G. F., "Modified Hilpert Correlation for Turbulent Convective Heat Transfer from a NACA Profile of Wind Turbine Blades," *AIAA 39th Thermophysics Conference*, AIAA, Reston, VA, 25–28 June 2007.

[30] Wang, X., Naterer, G. F., and Bibeau, E., "Convective Droplet Impact and Heat Transfer from a NACA Airfoil," *Journal of Thermophysics and Heat Transfer* (to be published).

[31] Wang, X., Naterer, G. F., and Bibeau, E., "Wind Tunnel Measurements of Convective Heat Transfer with Droplet Impact on a Wind Turbine NACA63-421 Blade," *ASME-JSME Thermal Engineering Conference and Summer Heat Transfer Conference*, ASME, New York, 8–12 July 2007.

[32] Montelpare, S., and Ricci, R., "A Thermographic Method to Evaluate the Local Boundary Layer Separation Phenomena on Aerodynamic Bodies Operating at Low Reynolds Number," *International Journal of Thermal Sciences*, Vol. 43, No. 3, 2004, pp. 315–329. doi:10.1016/j.ijthermalsci.2003.07.006

[33] Okong'o, N., and Knight, D. D., "Implicit Unstructured Navier-Stokes Simulation of Leading Edge Separation over a Pitching Airfoil," *Applied Numerical Mathematics*, Vol. 27, No. 3, 1998, pp. 269–308. doi:10.1016/S0168-9274(98)00012-9